

S. M. Dean · B. N. Lawrence · R. G. Grainger  
D. N. Heuff

## Orographic cloud in a GCM: the missing cirrus

Received: 13 September 2004 / Accepted: 25 February 2005 / Published online: 11 May 2005  
© Springer-Verlag 2005

**Abstract** Observations from the International Satellite Cloud Climatology Project (ISCCP) are used to demonstrate that the 19-level HadAM3 version of the United Kingdom Met Office Unified Model does not simulate sufficient high cloud over land. By using low-altitude winds, from the European Centre for Medium Range Weather Forecasting (ECMWF) Re-Analysis from 1979 to 1994 (ERA-15) to predict the areas of maximum likelihood of orographic wave generation, it is shown that much of the deficiency is likely to be due to the lack of a representation of the orographic cirrus generated by sub-grid scale orography. It is probable that this is a problem in most GCMs.

---

### 1 Introduction

It has been known since at least the 1940s (e.g. Queney 1948) that there are two conditions, which can lead to the formation of large orographic cirrus clouds. First, over high mountains strong winds can generate very large amplitude vertically propagating waves. The displacements in these waves can be large enough for ice crystals of significant size to grow in the rapid updrafts. Such crystals can be advected by the wind for long distances before they evaporate (for example, Hewson 1993, identified orographic cirrus clouds forming off Iceland and the Faeroe islands in otherwise clear air). Second, some regions of the troposphere are regularly

supersaturated with respect to ice but not with respect to water (Jenson et al. 2001). Any ice which is created due to ascent in an orographic wave will not evaporate when the air returns to its original level (Queney et al. 1960). The ability of small hills to produce significant cirrus clouds by this method was first identified by Ludlam (1952). Here, several case studies were presented which showed that ridges or hills in Britain of only about 300 m are able to vertically displace air in the upper troposphere by up to 700 m to produce large cirrus clouds. Similarly, Brown (1983) used observational research flights to show that orographic cirrus generated over Britain were caused by hydrostatic vertically propagating gravity waves. Conover (1964) pioneered the use of satellite imagery to study the size of orographic cirrus clouds and the nature of the waves that create them.

Orographic clouds are generated by orography at a wide-range of scales and thus take many forms. In this paper, we concentrate on orographic cirrus. Cirrus clouds in the upper troposphere play an important role in a number of aspects of the climate system. They not only have a direct radiative impact, but also influence the distribution of water vapour in the upper troposphere (e.g. Stephens 2002) and the potential for chemical processing of atmospheric constituents. Cold cirrus clouds are very effective at trapping outgoing longwave radiation and can also be strong reflectors of incoming shortwave radiation. Which process dominates is highly dependent on macrophysical properties such as the optical thickness of the cloud, which itself depends on microphysical properties such as the crystal size (Stephens et al. 1990). This uncertainty has consequences for studies of climate change. All GCM simulations of climate change agree that in a warmed atmosphere a more active hydrological cycle results in more transport of water vapour into the upper troposphere (Sundqvist 2002). Yet, the predictions of changes in cirrus amount, and whether there is a resulting positive or negative feedback on temperatures, vary widely.

---

S. M. Dean (✉) · R. G. Grainger  
Atmospheric Oceanic and Planetary Physics,  
Clarendon Laboratory, University of Oxford,  
Oxford, Oxfordshire, UK

B. N. Lawrence  
British Atmospheric Data Centre, Rutherford  
Appleton Laboratory, Chilton, Oxfordshire, UK

D. N. Heuff  
Department of Physics and Astronomy, University  
of Canterbury, Christchurch, New Zealand

DelGenio (2002) recognised that one of the reasons why cirrus clouds are such a large uncertainty in GCM simulations is that the dynamic processes that create cirrus are poorly resolved by current GCMs and are different in different parts of the globe. For example, scales smaller than the horizontal grid-box scale (typically of order one hundred to many hundreds of kilometres), are simply omitted. This missing subgrid orography causes a large part of the atmospheric response to the orography to be absent in GCMs. The dynamic effects of this missing response are typically addressed by the use of a gravity wave parameterisation (e.g. Palmer et al. 1986), but, as discussed above, it is obvious that the missing orography must also contribute to the presence of cirrus above and in the lee of orography.

This paper sets out to demonstrate that not only is at least one GCM (UK Met Office Unified Model, HADAM3) deficient in cirrus, but also that much of that deficiency is due to the lack of orographic cloud. This is done by predicting the areas where orographic cirrus might be thought to be more climatologically prevalent and comparing that to both observations and areas of model deficiencies. The prediction is carried out by assuming that climatological orographic cirrus will be present where large amplitude hydrostatic gravity waves would be commonly generated. As will be seen, the visual correlation between the areas of model deficiency and the prediction of large amplitude waves is good.

## 2 Predicting the location of orographic cirrus

There is a considerable history of the use of linear hydrostatic gravity wave theory to explain the presence of orographic clouds over large mountains (e.g. Reid 1975, in an explanation of orographic clouds over the mountain ranges of New Zealand). Durran (1986) showed that while orographic cirrus clouds generated by small amplitude waves could be described by linear theory, the formation of cloud can have a strong feedback into the vertical structure of the gravity wave. For large amplitude waves, other nonlinear effects become important and dynamical processes such as hydraulic jumps can occur.

To provide a simple estimate of where orographically driven wave processes may be important in generating cirrus, we use the orthogonality of the lower-level wind and a measure of sub-grid scale ridge direction to identify possible major gravity wave sources. The winds used are a 10-year subset from 1984 to 1993 of the 15 year European Centre for Medium Range Weather Forecasting (ECMWF) Re-Analysis project (ERA-15) (ECMWF 1995).

The six hourly winds are interpolated onto a regular  $2.5^\circ$  by  $2.5^\circ$  grid, and a “lower-level” wind is defined on that grid by selecting winds from the pressure-level closest to the mean orography (on that grid) plus half

the sub-grid orography in the direction of the wind. The height of the sub-grid orography is taken to be  $2\sigma^{\frac{1}{2}}$  where  $\sigma$  is the variance and is a function of the wind direction (see the Appendix). This method achieves a balance between the alignment of the orography and the height at which a near surface (non boundary layer) streamline is lifted over the orography.

## 2.1 Prediction results

Figure 1 is the climatological average of the component of the wind vector, which is perpendicular to the ridge alignment calculated from global six hourly ERA-15 winds. This indicates where ridges are aligned predominantly perpendicular to prevalent winds, and thus can be considered potential areas for orographic cirrus to form.

A number of mountain ranges and plateau edges are highlighted. The strongest forcings are seen over the Andes on the western edge of South America, and the Coastal and Rocky Mountain Range stretching through western Canada and the USA. Additional analysis has shown that many of the strongest features correspond to westerly winds. The ridge alignments predicted by this scheme are also in good qualitative agreement with those from the more complicated ridge-finding algorithm of Bacmeister (1993).

## 3 Climatological cirrus seen in the ISCCP analyses

The International Satellite Cloud Climatology Project (ISCCP) (Rossow and Schiffer 1999; Rossow et al. 1996) combines satellite-measured radiances in the visible and infrared, from up to five geostationary and two polar

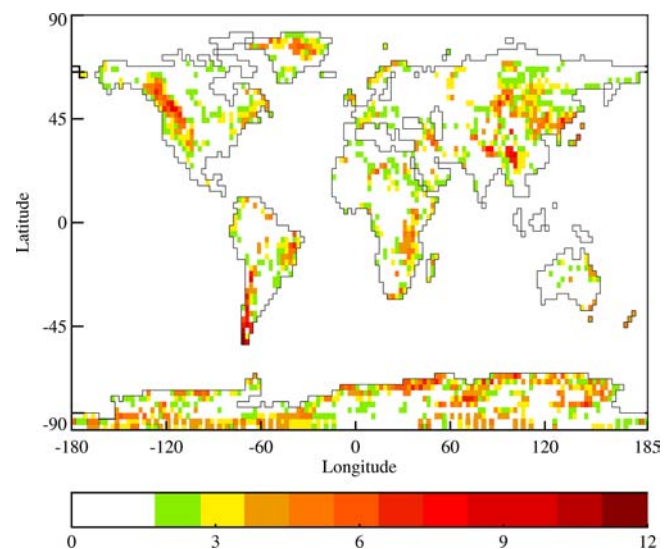


Fig. 1 Climatological average of the component of the wind vector perpendicular to the dominant ridge orientation ( $\text{ms}^{-1}$ )

orbiting satellites, with the TIROS Operational Vertical Sounder (TOVS) temperature–humidity datasets. Publicly available ISCCP data extend from 1983 until 2001 and more recent data continues to be made available.

The International Satellite Cloud Climatology Project observations include a cloud amount, which represents the percentage cloud cover, an optical depth and a cloud top pressure. From this information ISCCP is able to classify clouds into categories such as cirrus or cumulus. The definitions used by ISCCP can be seen in Fig. 2. While the minimum optical depth is displayed as zero, in practice the analysis is not sensitive enough to detect clouds with optical depths of less than 0.1. The six high and middle cloud types are also further subdivided into liquid and ice, leading to a total of 15 different cloud type categories. At night, ISCCP provides only a cloud amount and cloud top pressure.

The ISCCP algorithms used to derive cloud properties have undergone a number of modifications over time, including improved cloud detection. In particular, the ISCCP-D dataset, in comparison with the ISCCP-C dataset, has a lower threshold for the detection of thin cloud over orography and a more complicated model of the ice microphysical properties. This is important because it has been recognised that ISCCP-C is relatively poor at detecting thin upper tropospheric clouds. Jin et al. (1996) compared ISCCP C1 data with high-resolution infrared sounder (HIRS) cloud amounts and found that the HIRS dataset contained about 12% more cloud cover than ISCCP due to its higher sensitivity to thin cirrus. Liao et al. (1995) also found that, when compared to cloud data derived from the stratospheric aerosol and gas experiment (SAGE) II, ISCCP-C data

misses about 1/3 of high level clouds, most of which is very thin cirrus.

A number of studies have also been performed to compare the ISCCP results to models (e.g. Haskins et al. 1995; Jakob 1999). With cirrus this is difficult to do for two reasons: first, cirrus is defined as a cloud type which is optically thin, constituted of ice and with a top in the upper troposphere. ISCCP observations represent clouds as a single plane parallel layer in the atmosphere, and thus multiple overlying cloud decks are classified in height by only one of the layers. Thus, thin cirrus overlying thicker low-level cloud (as often happens when air is lifted over orography) could be erroneously classified as cirrostratus or deep convective. Second, the model data should ideally be sampled in the same way as the satellite observes the atmosphere (e.g. only during the same local times as seen by the satellite).

Webb et al. (2001) have compared the ISCCP C data with the Unified Model, ECMWF climate model and the Laboratoire de Météorologie Dynamique (LMD) atmospheric model. Their analysis focused on oceanic regions that represented different cloud regimes. Compared to ISCCP, they found too much high cloud over the tropical warm pool in the Unified Model, but too little over the midlatitude northern Pacific.

Fowler and Randall (1999) in an examination of upper-tropospheric clouds carried out a comparison of ISCCP-D data with the Colorado State University general circulation model. They found reasonable agreement except for cirrus ( $\tau < 3.6$ ), which was dramatically underpredicted. They also found that the model simulated upper tropospheric clouds in the tropics more successfully than at midlatitudes. They hypothesised that this was primarily caused by the model's failure to simulate upper tropospheric clouds over the continents, especially over high plateaus and mountain ranges.

Weare (2004) compared the variability in ISCCP-D cloud amounts and ice/water paths to “ISCCP-like” model results from the Atmospheric Model Intercomparison Project using monthly mean layer cloud amounts. The models considered were found to capture moderately well the variability observed in the ISCCP-D data.

In the next section, we present an analysis of high cloud in a 10-year ISCCP D2 dataset (1984–1993) on a  $2.5^\circ$  grid. To remain consistent with the ISCCP definitions (Fig. 2), we define high cloud as cloud above 440 hPa, and cirrus as that proportion of high cloud with  $0.1 < \tau < 3.6$ .

### 3.1 ISCCP orographic cirrus: results

Figure 3 is the climatological global cirrus cloud amount (percentage of a grid box covered by cloud). There are two key features: the 30–40% cloud cover seen over the equatorial Indian and Eastern Pacific Oceans, most of which are likely to be from the detection of large anvils created at the top of convective towers, and the increase

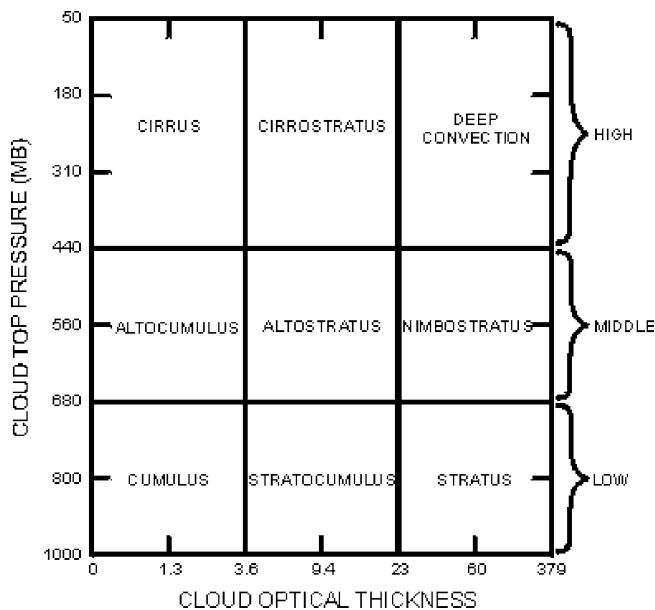
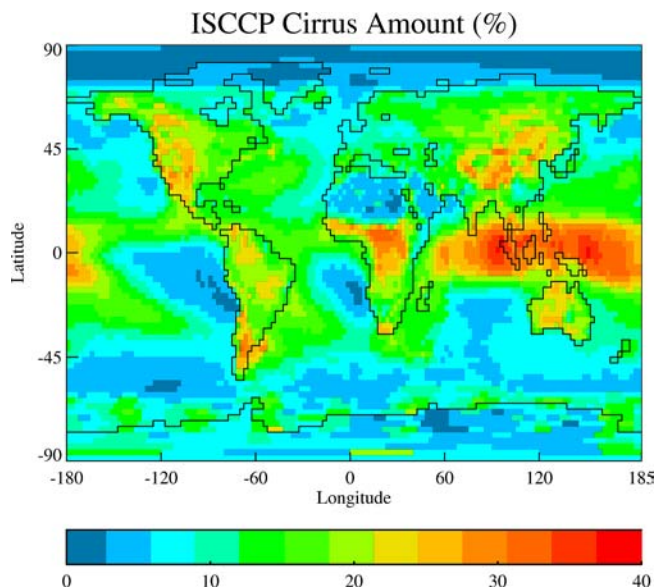


Fig. 2 Cloud types as defined by optical depth and cloud top pressure for the ISCCP cloud dataset. From <http://isccp.giss.nasa.gov/>



**Fig. 3** Global climatological ISCCP cirrus cloud amount (percent of a grid box covered in cloud) for the years 1984–1993

in cirrus seen over much of the world's orography, when compared to the surrounding oceans. It is the latter which is of interest here.

Over nearly all land areas, except for North Africa and Antarctica, there is more cirrus over the land than the adjacent ocean. Identification of orographic cirrus is difficult in areas where cirrus might be generated by convection or frontal lifting. However, by looking at the ISCCP total high cloud (Fig. 4) as well as cirrus, it is possible to gain further insight: optically thick convective towers will be detected in conjunction with anvil cirrus. Additionally, there is an a priori expectation that

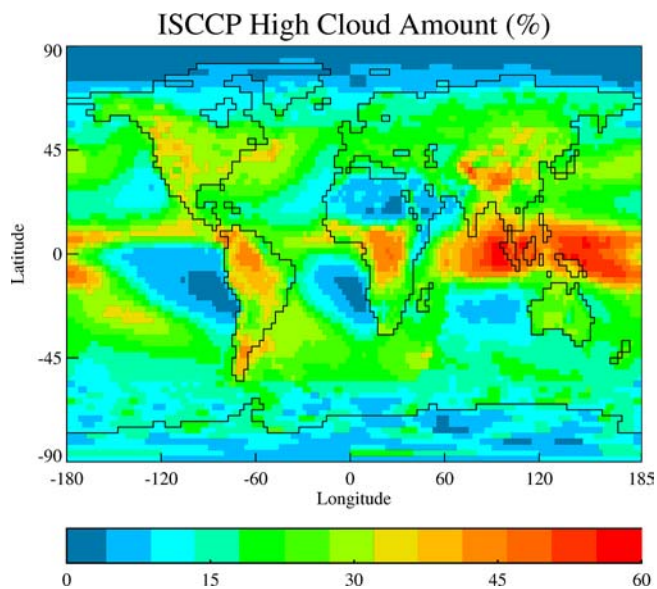


**Fig. 4** Global climatological ISCCP total high cloud amount for the years 1984–1993

orographic cirrus should occur over and adjacent to the areas identified earlier. Further, the Atlantic and Pacific storm tracks allow us to estimate that the midlatitude frontal cirrus contribution will be of order 18%. Figure 4 is comparable to results presented in Weare (2004).

As noted by Rossow and Schiffer (1999), cloud detection errors are high at polar latitudes for the ISCCP dataset. This is because there is usually a snow surface with a similar reflectivity to clouds, cold temperatures, no geostationary data, and low solar illuminations. Therefore, we do not attempt to interpret the ISCCP results at high latitudes.

Of the major areas of cirrus above land, the two areas of central South America and central Africa show cirrus amounts of 30% and 40%, respectively. The most likely source of this cirrus is convective anvils, as these are equatorial and associated with areas of optically thick cloud. By contrast, North America is another area of cirrus where the large land mass might be expected to contribute some convective activity. However, the largest component of high cloud in this region is cirrus and there are considerable gravity wave sources (Fig. 1). This is suggestive of both strong orographic and convective cirrus influences.

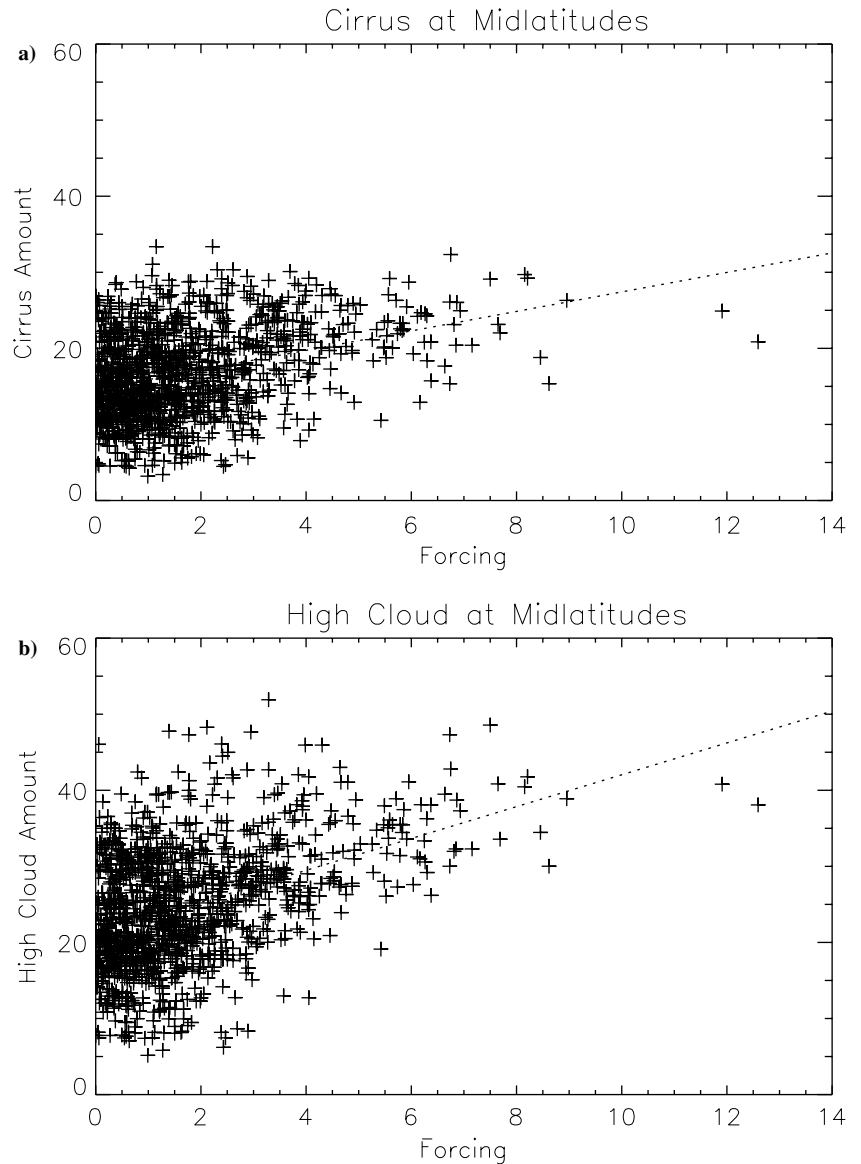
The lower latitudes of South America also show high amounts of cirrus over both the orography and the adjacent ocean. The strong gravity wave sources in the ERA analysis suggest that a significant proportion of this cirrus could be orographic in origin. The oceanographic cirrus could potentially be caused by ice crystals advected by the predominantly westerly winds.

Over the Himalayas, and Asia generally, it is difficult to attribute unambiguously the high levels of cirrus to orographic processes. It seems likely that both orographic and convective processes may be happening. An analysis of the seasonal changes has shown that the monsoon plays a role in the high cloud amounts. In addition, it is quite possible that high cirrus clouds in this region form in association with low level cloud, leading to the reclassification of the cirrus as optically thick. Small changes in cirrus over northern Asia and the tip of South Africa are more easily linked to gravity waves.

The results from extra-tropical Australia, where there are cirrus amounts of 20–30%, do not fit with the source-analysis concept. Australia, much like northern Africa, is primarily desert and has only small mountain ranges, mostly in the east. Given that the high cloud in this region is made up almost entirely of thin cirrus, and has a summer maximum, it is likely that weak convection (or climatologically synoptic weak lifting) in a moisture sparse environment is responsible for the cirrus.

While the maps provide a qualitative view of the relationship between forcing and cirrus, a more quantitative view is also possible. Figure 5 shows the ISCCP cirrus amount in (a), and the high cloud amount in (b) as a function of the orographic forcing parameter. A best fit straight line is indicated, though there is no expecta-

**Fig. 5 a** Climatological average of the component of the wind perpendicular to the dominant ridge orientation plotted against the ISCCP climatological cirrus amount from two 25° bands taken from Northern and Southern midlatitudes (65.5°–32.5°North and 25°–60°South). **b** As for **a** but for total high cloud



tion that the data should necessarily fit such a line. It is simply used to emphasise that at midlatitudes, there is a weak trend associating higher forcings with increased amounts of cirrus and high cloud. The difference in the strength of the relationship between forcing and cloud amount for cirrus and high cloud is consistent with downwind advection of cirrus. Transport of ice away from mountains results in a decorrelation between forcing and cirrus amount.

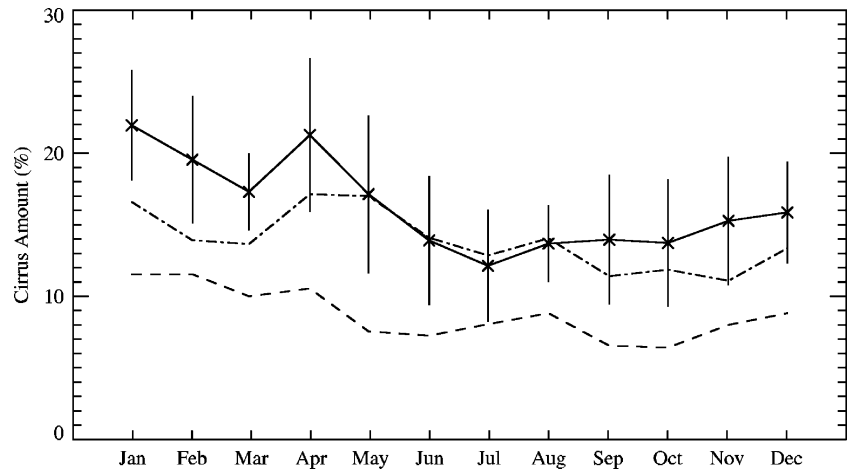
It is difficult to interpret from Fig. 3, whether there are any changes in cirrus for narrower midlatitude mountain ranges of large to moderate forcing, such as those of New Zealand and Scandinavia. New Zealand has previously been identified as having a significantly greater amount of cirrus cover than the surrounding ocean by Uddstrom et al. (2001) and as such is now used as a case study for closer investigation. New Zealand's alignment perpendicular to prevalent north westerly airflows ensures large scale gravity wave activity, while

its narrow high land mass located at midlatitudes minimises any influences from convective activity. Thus the interpretation of any increases in cirrus over orography is much simpler when compared to larger land masses.

The solid line in Fig. 6 is the climatological cirrus amount for each month over a New Zealand land point. The dashed line is for the adjacent sea point to the west and the dash-dot line for the adjacent sea point to the east. The vertical bars on the solid line indicate one standard deviation either side of the mean. The standard deviation is calculated from the 10 months used for each data point.

In all months, there is a considerable increase in cirrus between the westward point and the land point, with a maximum change of 12 (120% increase) seen in April and a minimum of 4 (44% increase) seen in July. An increase is also seen for the eastward point, which is about half that of the land point in summer, and about

**Fig. 6** Monthly climatological cirrus amount for a New Zealand land point (*solid line*) and the adjacent sea points to the west (*dashed line*) and east (*dash-dot line*) from the ISCCP D data. Vertical bars on the land data indicate one standard deviation either side of the mean



the same in winter. All three points tend to have slightly higher cirrus amounts during the summer when compared to winter. An analysis of ERA15 has shown that the winds are predominantly in the mean strong westerlies in all months. As such, a simple conceptual model to explain this cirrus trend is that ice forms rapidly in the upper troposphere over the New Zealand mountains in large scale uplifting by gravity waves, before slower growth and eventual evaporation as the ice is advected downwind. Additional investigations have shown that the increase in cirrus regularly persists for up to four gridboxes east of New Zealand ( $\approx 800$  km).

In conclusion, both for large mountain ranges and smaller narrower ranges there is considerable evidence that gravity wave activity plays an important role in creating cirrus over midlatitude land masses.

#### 4 The unified model

The high cloud cover in a 10 year simulation of the United Kingdom Met Office's (UKMO) climate version of the Unified Model will now be discussed. Known as HadAM3 this model has a  $2.5^\circ$  by  $3.75^\circ$  resolution and 19 levels in the vertical. This configuration is an atmosphere-only model and has prescribed sea surface temperatures. A full description of the model can be found in Pope et al. (2000). The simulation included the 2B mixed phase precipitation scheme with a prognostic ice variable as described by Wilson and Ballard (1999). In this configuration ice is advected by the model's tracer advection scheme and allowed to grow and decay through physical transfer equations. In theory, this should allow for the creation and survival, at least microphysically, of orographic cirrus clouds.

In order to compare the model simulations in a consistent way with ISCCP data, special diagnostics were incorporated into the Unified Model. This "ISCCP simulator" is that used by Webb et al. (2001) and the diagnostics attempt to mimic a satellite by observing the cloud from the top of the model domain. Through the

impact on the radiances, the diagnostics calculate an optical depth in association with a cloud amount. The diagnostics are thus a part of the radiation code, rather than the normal cloud subroutine, and only return values for the part of the Earth, which is illuminated by the Sun. For this study, the lower optical depth threshold for cirrus was set to 0.1, which is the published sensitivity threshold for ISCCP data over ocean.

#### 5 Results

Figure 7a is the difference between the climatological annual mean cirrus amount simulated by the model and that observed by ISCCP. To calculate this difference, the UM data has been interpolated onto the  $2.5^\circ$  by  $2.5^\circ$  ISCCP grid. To aid in considering the magnitude of these changes, and for future reference, Fig. 7b is the actual cirrus amount simulated in the control run.

Clearly, the differences are dominated by the lack of cirrus (blue) over North America, the bottom half of South America, the tip of southern Africa, central Asia and Australia. In general, there is a lack of cirrus of between 5% and 10% over most land and over some ocean areas, particularly to the east of the continents. Even at this low resolution one New Zealand gridbox can be seen to have too little cirrus. There is an excess of about 5% cirrus amount, in the tropical warm pool.

In a similar way, Fig. 7c, d presents the high cloud difference and values. There is too much high cloud over many of the world's oceans, especially for the Southern Ocean and the tropics. However, there is still not enough cloud in many of the land areas in which cirrus was missing. The magnitude of the deficiency in high cloud implies that it is caused predominantly by a lack of cirrus (cf. Fig. 7b). However, considering the model's predisposition to excess high cloud elsewhere, there is probably a contribution from a lack of optically thick cloud as well. The possibility of the model annual mean relative humidity simply being deficient at midlatitudes

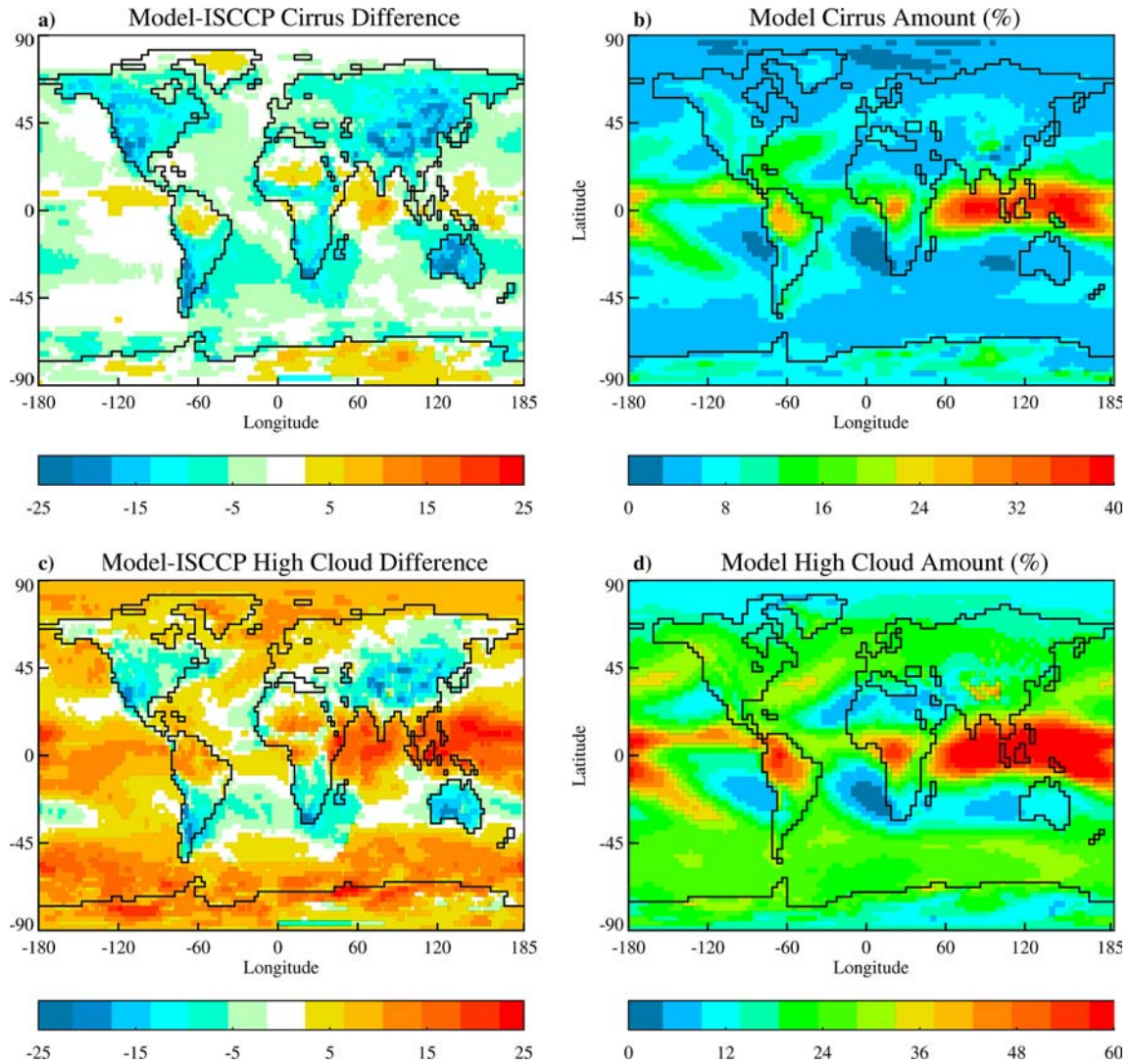


**Fig. 7** a Difference in the 10-year climatological cirrus amounts for the Unified Model and ISCCP. b The Unified Model 10 year climatological cirrus amount. c, d As for a and b but for total high cloud

has been rejected by comparison to the ERA-15 relative humidities.

The excess in tropical high cloud seems to be associated with areas of strong convection. Analysis of the model’s standard high cloud diagnostic, which is output over the entire globe simultaneously, has indicated that, compared with ISCCP data, the model is producing too much convective cloud during daytime hours, but compensates with too little at night. The anomalous pattern of increased cirrus amount seen at 70°S has been identified in the D2 dataset previously by Norris (2000).

Model cirrus amounts for the same three gridboxes as discussed in Fig. 6, are presented in Fig. 8. These are lowest over the land point, about a third of the observed cirrus over New Zealand. Cirrus is increased to the east but remains well below the observed amounts. An increase is seen in high cloud over the land (not shown) suggesting that the resolved dynamics and/or upwind humidity profiles are only capable of producing optically thick cloud over orography. For comparison, simula-

tions conducted using the 31 level version of the Unified Model, which primarily gives increased resolution in the upper troposphere, gave no improvement to the model results presented here.

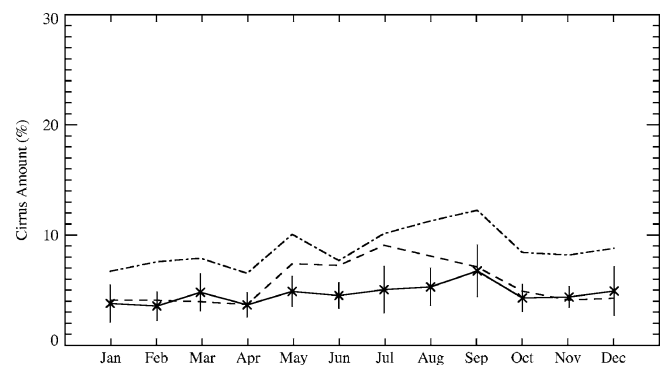


**Fig. 8** Cirrus amounts as for Fig. 6 but from a 10-year Unified Model integration

## 6 Conclusion

A number of areas of potential gravity wave activity have been identified using ERA-15 reanalysis winds and a topographic dataset. These are areas in which orographic cirrus has the potential to form. However, there are limits to the interpretation of these results. For instance, atmospheric stability has a profound effect on whether gravity waves are able to propagate vertically, and the distribution of water vapour in the upper troposphere will have a strong impact on any subsequent cloud formation. Thin cirrus clouds can be generated from both small and large mountain ranges by weak winds if the atmospheric humidity is high enough. Such weak winds will not appear very prominently in this analysis.

In general, the ISCCP analysis showed significant increases in cirrus over land compared to the oceans. Many of the largest increases at midlatitudes showed a good qualitative correlation with areas of gravity wave forcing identified by the ERA analysis, which picked out many of the Earth's major mountain ranges. Over and downwind of New Zealand, there was a significant increase in cirrus at all times of the year. Despite this, the increases over New Zealand were not prominent in the global comparisons, highlighting that at midlatitudes increases in orographic cirrus cover may be widespread.

A 10-year Unified Model simulation was found to dramatically underpredict cirrus (a deficiency of up to 25% cloud amount) over some midlatitude mountain ranges and by a lesser amount (5–10% cloud amount) over continents in general. While it was also found that there was an excess of up to 25% total high cloud amount over much of the world's oceans, a deficiency in high cloud remained over land, primarily due to the missing cirrus component. This was despite the inclusion of a prognostic ice variable capable of being advected by the model winds. Analysis over New Zealand suggested that the model does not currently produce extra cirrus over the land, or significantly in the lee.

Overall, these results suggest that the Unified Model is lacking in cirrus over major mountain ranges, and we assert that some part of this is due to the absence of subgrid gravity waves. This fault is also likely to be present in other climate models.

Papers such as Kaercher and Lohman (2002) have already shown that cirrus nucleation can be parameterised in GCMs as a function of the vertical velocity. Our work suggests that the large vertical velocities associated with sub-grid orographic gravity waves must be included in GCMs to better simulate midlatitude cirrus clouds. Future work is focused on utilising GCM gravity wave parameterisations to compensate for some of this discrepancy.

**Acknowledgements** The ISCCP data were obtained from the NASA Langley Research Center Atmospheric Sciences Data Center. The

ERA-15 Re-analysis data were obtained from the United Kingdom Meteorological Office through the British Atmospheric Data Centre. This work was partially funded by the Marsden Fund of the Royal Society of New Zealand, and the NERC thematic programme Clouds Water Vapour and Climate. The authors would like to thank Steve Eckermann for his helpful comments on this work.

## 7 Appendix

The average valley to peak height of subgrid orography is taken to be about  $2\sigma^2$ , where  $\sigma$  is the variance of all the subgrid orography about the gridbox mean height. However, because orography preferentially aligns as ridges, simply using a total variance would greatly underestimate or overestimate the true surface wave amplitude (depending on the surface wind direction). It is more useful to construct a variance function, which describes the amount of variance in any given wind direction. The maximum in such a variance function then represents the dominant subgrid ridge alignment. In this paper, this is done using subgrid gradients calculated from the US Navy 10' topographical dataset and a modification of the spectrum function ideas used by the Unified Model gravity wave scheme described in Palmer et al. (1986). A full derivation follows.

Consider an isolated mountainous region within a rectangle defined by  $0 < x < X$  and  $0 < y < Y$ , with  $h(x, y)$  the height of the orography minus the mean elevation.  $h(x, y)$  is also set equal to zero at all points outside the rectangle. Then the variance of the orography is simply

$$\sigma = \int_0^Y \int_0^X \frac{(h(x, y))^2}{XY} dx dy \quad (1)$$

Using Parseval's theorem, this becomes

$$\sigma = \frac{4\pi^2}{XY} \int_{-\infty}^{\infty} \int_{-\infty}^{\infty} |\hat{h}(k, l)|^2 dk dl, \quad (2)$$

which can be re-written as

$$\sigma = \int_{-\infty}^{\infty} \int_{-\infty}^{\infty} S(k, l) dk dl \quad (3)$$

where

$$S(k, l) = \frac{4\pi^2}{XY} |\hat{h}(k, l)|^2 \quad (4)$$

is a spectrum function of orographic height variance. Finally, it is more useful to write the spectrum function in terms of polar coordinates where  $k = \kappa \cos \chi$  and  $l = \kappa \sin \chi$  so that

$$\sigma = \int_{\kappa_L}^{\kappa_U} \int_0^{2\pi} \kappa S(\kappa, \chi) d\kappa d\chi \quad (5)$$

Here,  $\kappa$  has been restricted to the range of wave numbers between an upper ( $\kappa_U$ ) and a lower ( $\kappa_L$ ) that are of relevance for the forcing of gravity waves.

The Unified Model assumes that the spectrum can be separated in azimuth and wavenumber and that the wavenumber component of the spectrum function could fit a power law of the form

$$S(\kappa) = \kappa_0 \kappa^\gamma \quad (6)$$

where  $\kappa_0$  is a constant coefficient. The Unified Model chooses, based on observations, to use  $\gamma = -1.5$  and an azimuth dependence to account for anisotropy. This variance spectrum is defined as

$$\kappa S(\kappa, \chi) = \left(\frac{\mu}{\kappa}\right)^{1.5} (a \cos^2 \chi + 2b \sin \chi \cos \chi + c \sin^2 \chi) \quad (7)$$

where  $\mu = \kappa_0^{-1.5}$  is a constant coefficient and with  $b^2 < ac$ ,  $a > 0$  and  $c > 0$  to ensure positivity. The coefficients  $a$ ,  $b$  and  $c$  can be rewritten in terms of the squared gradients of the topography, defined as

$$\sigma_{xx} = \frac{1}{XY} \int_0^X \int_0^Y \left(\frac{\partial h}{\partial x}\right)^2 dx dy \quad (8)$$

$$\sigma_{xy} = \frac{1}{XY} \int_0^X \int_0^Y \left(\frac{\partial h}{\partial x}\right) \left(\frac{\partial h}{\partial y}\right) dx dy \quad (9)$$

$$\sigma_{yy} = \frac{1}{XY} \int_0^X \int_0^Y \left(\frac{\partial h}{\partial y}\right)^2 dx dy \quad (10)$$

From the definition of the Fourier transform and once again Parseval's theorem, it can be shown that for  $\sigma_{xx}$

$$\sigma_{xx} = \int_{\kappa_L}^{\kappa_U} \int_0^{2\pi} \kappa^3 \cos^2 \chi S(\kappa, \chi) d\kappa d\chi \quad (11)$$

Substituting for  $\kappa S(\kappa, \chi)$  and integrating leads to

$$\sigma_{xx} = \frac{\pi}{6} \mu^{1.5} (\kappa_U^{1.5} - \kappa_L^{1.5}) (3a + c) \quad (12)$$

Similar arguments lead to

$$\sigma_{xy} = \frac{\pi}{3} \mu^{1.5} (\kappa_U^{1.5} - \kappa_L^{1.5}) b \quad (13)$$

$$\sigma_{yy} = \frac{\pi}{6} \mu^{1.5} (\kappa_U^{1.5} - \kappa_L^{1.5}) (a + 3c) \quad (14)$$

Thus, combining Eqs. 12, 13 and 14,  $a$ ,  $b$  and  $c$  can be eliminated from Eq. 7 to give

$$\kappa S(\kappa, \chi) = \frac{3A}{4\pi \kappa^{1.5} (\kappa_U^{1.5} - \kappa_L^{1.5})} \quad (15)$$

where  $A$  is the anisotropy term

$$A = (4\cos^2 \chi - 1)\sigma_{xx} + (4\sin^2 \chi - 1)\sigma_{yy} + 8\sigma_{xy} \sin \chi \cos \chi \quad (16)$$

This result can be used in Eq. 5, to express the variance as

$$\sigma = \int_{\kappa_L}^{\kappa_U} \int_0^{2\pi} \frac{3A}{4\pi \kappa^{1.5} (\kappa_U^{1.5} - \kappa_L^{1.5})} d\kappa d\chi \quad (17)$$

Upon integrating with respect to  $\kappa$ , the variance as a function of  $\chi$  is found to be

$$\sigma(\chi) = \frac{3A(\kappa_U^{-0.5} - \kappa_L^{-0.5})}{2\pi(\kappa_U^{1.5} - \kappa_L^{1.5})} \quad (18)$$

The constant coefficient part of Eq. 18 is

$$C = \frac{3(\kappa_U^{-0.5} - \kappa_L^{-0.5})}{2\pi(\kappa_U^{1.5} - \kappa_L^{1.5})} \quad (19)$$

In line with the approach taken by the Unified Model, this constant coefficient is treated as tunable; however, its value does not affect the calculation of the direction of maximum variance as used in this paper.

To show how the squared gradients, defined in Eqs. 8, 9 and 10 are calculated from heights,  $h(x, y)$ , in the 10' US Navy topographical dataset, an illustration is useful:

o1	o2	o	o
•1	•	•	
o3	o4	o	o
•2	•	•	
o5	o6	o	o

In the above pattern, the points o are the 10' dataset points and thus  $\frac{\partial h}{\partial x}$  at point •1 is given by simple finite differencing as

$$\frac{\partial h}{\partial x} = \frac{1}{2} \times \left[ \frac{(h(o2) - h(o1))}{\Delta x} + \frac{(h(o4) - h(o3))}{\Delta x} \right] \quad (20)$$

$\frac{\partial h}{\partial y}$  is simply the north–south rather than the east–west calculation. The orographic gradients are calculated at all • points. The final value for the model grid is then simply the mean of all the values that lie within a model grid box.

## References

- Bacmeister JT (1993) Mountain wave drag in the stratosphere and mesosphere inferred from observed winds and a simple mountain wave parameterization scheme. *J Atmos Sci* 50(3):377–399
- Brown PRA (1983) Aircraft measurements of mountain waves and their associated momentum flux over the British Isles. *QJR Meteorol Soc* 109:849–865
- Conover JH (1964) The identification of orographically induced clouds observed by TIROS satellites. *J Appl Meteorol* 13:226–234
- DelGenio AD (2002) GCM simulations of cirrus for climate studies. In: Lynch DK, Sassen K, Starr DOC, Stephens G (eds) *Cirrus*. Oxford University Press, Oxford, pp 310–326
- Durran DR (1986) Mountain waves. In: Ray PS (eds) *Mesoscale meteorology and forecasting*. American Meteorological Society, Boston, pp 472–492
- ECMWF (1995) *User Guide to ECMWF Products 2.1*, European Centre for Medium-Range Weather Forecasting
- Fowler LD, Randall DA (1999) Simulation of upper tropospheric clouds with the Colorado State University general circulation model. *J Geophys Res* 104(D6):6101–6121

- Haskins RD, Barnett TP, Meyer Tyree M, Roeckner E (1995) Comparison of cloud fields from atmospheric general circulation model, in situ and satellite measurements. *J Geophys Res* 100 (D1):1367–1378
- Hewson TD (1993) Orographic cirrus generated by Iceland and the Faeroe Islands, 4–6 May 1993. *Meteorol Mag* 122:249–253
- Jakob C (1999) Cloud Cover in the ECMWF Reanalysis. *J Clim* 12:947–959
- Jenson EJ, Toon OB, Vay SA, Ovarlez J, May R, Bui TP et al (2001) Prevalence of ice-supersaturated regions in the upper troposphere: implications for optically thin ice cloud formation. *J Geophys Res* 106(D15):17253–17266
- Jin Y, Rossow WB, Wylie DP (1996) Comparison of the climatologies of high-level clouds from HIRS and ISCCP. *J Clim* 9:2850–2879
- Kaercher B, Lohmann U (2002) A parameterization of cirrus cloud formation: homogeneous freezing of supercooled aerosols. *J Geophys Res* 107(D2):AAC4-1–AAC4-10
- Liao X, Rossow WB, Rind D (1995) Comparison between SAGEII and ISCCP high level clouds I, global and zonal mean cloud amounts. *J Geophys Res* 100(D1):1121–1135
- Ludlam FH (1952) Orographic cirrus clouds. *QJR Meteorol Soc* 78(338):552–562
- Norris JR (2000) What can cloud observations tell us about climate variability. *Space Sci Rev* 94:375–380
- Palmer TN, Shutts GJ, Swinbank R (1986) Alleviation of a systematic westerly bias in general circulation and numerical weather prediction models through an orographic gravity wave drag parameterization. *QJR Meteorol Soc* 112:1001–1039
- Pope VD, Gallani ML, Rowntree PR, Stratton RA (2000) The Impact of new physical parameterizations in the Hadley Centre climate model: HadAM3. *Clim Dyn* 16:123–146
- Queney P (1948) The problem of airflow over mountains: a summary of theoretical studies. *Bull Am Met Soc* 29:16–26
- Queney P, Corby G, Koshmieder NGH, Zierep J (1960) The influence of mountains on the atmosphere. WMO Tech Note No. 34
- Reid SJ (1975) Long-wave orographic clouds seen from satellites. *Weather* 30:117–123
- Rossow WB, Schiffer RA (1999) Advances in understanding clouds from ISCCP. *Bull Am Met Soc* 80(11):2261–2287
- Rossow WB, Walker AW, Beuschel DE, Roiter MD (1996) International satellite cloud climatology project (ISCCP) documentation of new cloud datasets, World Climate Research Programme
- Stephens GL (2002) Cirrus, climate, and global change. In: Lynch DK, Sassen K, Starr DOC, Stephens G (eds) *Cirrus*. Oxford University Press, Oxford, pp 433–448
- Stephens GL, Tsay SC, Stackhouse PW, Flatau PJ (1990) The relevance of microphysical and radiative properties of cirrus clouds to climate and climate feedback. *J Atmos Sci* 47(14):1742–1753
- Sundqvist H (2002) Cirrus modelling for general circulation and climate models. In: Lynch DK, Sassen K, Starr DOC, Stephens G (eds) *Cirrus*. Oxford University Press, Oxford, pp 297–309
- Uddstrom MJ, McGregor JA, Gray WR, Kidson JW (2001) A high resolution analysis of cloud amount and type over complex orography. *J Appl Meteorol* 40:16–33
- Weare BC (2004) A comparison of AMIP II model cloud layer properties with ISCCP D2 estimates. *Clim Dyn* 22:281–292
- Webb M, Senior C, Bony S, Morcrette JJ (2001) Combining ERBE and ISCCP data to assess clouds in the Hadley Centre, ECMWF and LMD atmospheric climate models. *Clim Dyn* 17(12):905–922
- Wilson DR, Ballard SP (1999) A microphysically based precipitation scheme for the UK Meteorological Office Unified Model. *QJR Meteorol Soc* 125:1607–1636